Umling Natalie Elizabeth (Orcid ID: 0000-0001-9999-1737)
Oppo Delia W. (Orcid ID: 0000-0003-2946-5904)
Yu Jimin (Orcid ID: 0000-0002-3896-1777)
Yan Mi (Orcid ID: 0000-0003-4730-3781)
Gebbie Geoffrey (Orcid ID: 0000-0003-0846-0338)
Lund David C (Orcid ID: 0000-0002-4847-2889)
Huang Kuo-Fang (Orcid ID: 0000-0002-7858-4865)
Costa Karen Badaraco (Orcid ID: 0000-0002-4757-0524)

Atlantic circulation and ice sheet influences on upper South Atlantic temperatures during the last deglaciation

N.E. Umling[1,2*], D.W. Oppo[1], P. Chen[3], J., Yu[3], Z. Liu[4], M. Yan[5,6], G. Gebbie[7], D. C. Lund[8], K. R. Pietro[1], Z.D. Jin[9], K.-F. Huang[1,10] K.B. Costa[11], F.A.L. Toledo[11]

[1]Department of Geology and Geophysics, Woods Hole Oceanographic Institution, Woods Hole, MA 02543, USA
[2]Present address: Department of Earth and Planetary Sciences, American Museum of Natural History, Central Park West at 79th Street, New York, NY 10024-5192, USA
[3]Research School of Earth Sciences, The Australian National University, Canberra, ACT 0200, Australia
[4]Department of Geography, Ohio State University, Columbus, OH 43210, USA
[5]Key Laboratory of Virtual Geographic Environment, Ministry of Education, State Key Laboratory of Geographical Environment Evolution, Jiangsu Provincial Cultivation Base; School of Geography Science, Nanjing Normal University, Nanjing 210023, China
[6]Jiangsu Center for Collaborative Innovation in Geographical Information Resource Development and Application, Nanjing 210023, China
[7]Department of Physical Oceanography, Woods Hole Oceanographic Institution, Woods Hole, MA 02543, USA
[8]Department of Marine Sciences, University of Connecticut, Storrs, Connecticut, USA
[9]State Key Laboratory of Loess and Quaternary Geology, Institute of Earth Environment, Chinese Academy of Sciences, Xi'an, China
[10]Institute of Earth Sciences, Academia Sinica, Taipei 11529, Taiwan
[11]Oceanographic Institute, University of São Paulo, São Paulo, CEP 05508-900, Brazil

[*]Corresponding author: Natalie Umling (numling@amnh.org)

Key Points:

- Western South Atlantic waters between 1.1 and 1.9 km warmed by ~2.5-3.0 °C from the LGM to the Holocene.
- Deglacial subsurface warming continued into the Bølling-Allerød, after Atlantic Meridional Overturning Circulation had recovered.
- The demise of ice sheets likely prevented a return to cooler temperatures during the Bølling-Allerød

This article has been accepted for publication and undergone full peer review but has not been through the copyediting, typesetting, pagination and proofreading process which may lead to differences between this version and the Version of Record. Please cite this article as doi: 10.1029/2019PA003558

Abstract

Atlantic Meridional Overturning Circulation (AMOC) disruption during the last deglaciation is hypothesized to have caused large subsurface ocean temperature anomalies, but records from key regions are not available to test this hypothesis, and other possible drivers of warming have not been fully considered. Here, we present the first reliable evidence for subsurface warming in the South Atlantic during Heinrich Stadial 1 (HS1), confirming the link between large-scale heat redistribution and AMOC. Warming extends across the Bølling-Allerød (BA) despite predicted cooling at this time, thus spanning intervals of both weak and strong AMOC indicating another forcing mechanism that may have been previously overlooked. Transient model simulations and quasi-conservative water-mass tracers suggest that reduced northward upper ocean heat transport was responsible for the early deglacial (HS1) accumulation of heat at our shallower (~1,100 m) site. In contrast, the results suggest that warming at our deeper site (~1,900 m) site was dominated by southward advection of North Atlantic mid-depth heat anomalies. During the BA, the demise of ice sheets resulted in oceanographic changes in the North Atlantic that reduced convective heat loss to the atmosphere, causing subsurface warming that overwhelmed the cooling expected from an AMOC reinvigoration. The data and simulations suggest that rising atmospheric CO_2 did not contribute significantly to deglacial subsurface warming at our sites.

1. Introduction

Abundant evidence exists that the Atlantic Meridional Overturning Circulation (AMOC) weakened episodically during the last glacial and deglacial periods, perhaps because massive icebergs surging from continental ice sheets and melting across the subpolar North Atlantic increased surface buoyancy and disrupted the conversion of surface to deep water (Broecker et al., 1985; Bond et al., 1992; Clark et al., 2002). Model simulations suggest that an AMOC collapse would result in reduced heat loss through convective exchange in the North Atlantic (Galbraith et al., 2016), trapping heat in the North Atlantic subsurface (Galbraith et al., 2016; Liu et al., 2009; Marcott et al., 2011; Pedro et al., 2018; Zhang et al., 2017), some of which would be transported southward along the deep western boundary current and contribute to warming at mid-depths (1.5-2.5 km) of the South Atlantic (Galbraith et al., 2016; Liu et al., 2009; Marcott et al., 2011; Pedro et al., 2018; Zhang et al., 2017). Heat also accumulates in the South Atlantic thermocline due to reduced northward upper ocean heat transport (Galbraith et al., 2016; Liu et al., 2009; Marcott et al., 2011; Pedro et al., 2018; Zhang et al., 2017). Upon AMOC resumption, North Atlantic subsurface heat is released to the atmosphere and renewed subduction of NADW transports cold, salty waters to the South Atlantic (Pedro et al., 2018). In the simulations, the South Atlantic thermocline also cools due to renewed strong northward upper ocean flow.

Heinrich stadial 1 (HS1; ~17.5-14.7 kyr BP) is a key period associated with evidence for a weakened AMOC (Clark et al., 2002; Lynch-Stieglitz et al., 2014; McManus et al., 2004) and the onset of deglacial atmospheric CO_2 rise (Monnin et all., 2001). The end of HS1 is associated with evidence for an abrupt AMOC recovery and rapid warming in the North Atlantic region (McManus et al., 2004; Weldeab et al., 2016), culminating in the Bølling-Allerød (BA;14.7-13.0 kyr BP) warm period. The interval encompassing these two events is the ideal target for initial studies of the effect of a reduced AMOC on South Atlantic

subsurface temperatures and other potential forcings of subsurface temperature change. Comparisons to earlier and later events of more modest AMOC decline and recovery may also help clarify the strength of the link between AMOC and South Atlantic subsurface temperature (Lynch-Stieglitz et al., 2014; Them et al., 2015).

Previous studies suggest HS1 warming occurred in the intermediate (1.2-1.4 km; Marcott et al., 2011; Weldeab et al., 2016; Thiagarajan et al., 2014) and mid (1.8-2.6 km; Roberts et al., 2016) depths of the North Atlantic, as well as the intermediate depth (0.6-0.85 km; Poggemann et al., 2018; Roberts et al., 2016) and deep South Atlantic (3.8 km; Roberts et al., 2016). However, aside from a single deep-sea coral clumped isotope record (Thiagarajan et al., 2014), intermediate and deep water temperatures in these previous studies were estimated using the magnesium/calcium ratios (Mg/Ca) of benthic foraminifera. Yet several studies suggest that Mg/Ca of benthic foraminifera is influenced by carbonate chemistry, an effect that is generally obscured in core top calibrations by the positive relationship between bottom water temperature and carbonate ion saturation (Elderfield et al., 2006; Rosenthal et al., 2006; Yu and Elderfield, 2008). While it is often assumed that benthic foraminifera living within the sediment (infaunal habitat) are not exposed to fluctuations in carbonate ion saturation and can be used to reconstruct temperature (Elderfield et al., 2010), recent evidence suggests this assumption is incorrect (Weldeab et al., 2016). Pairing measurements of Mg/Ca and lithium/calcium ratios (Li/Ca) appears to eliminate much of the bias associated with changes in carbonate chemistry (Bryan and Marchitto, 2008; Marchitto et al., 2018). In particular, Mg/Li in the aragonitic foraminifera *Hoeglundina elegans* appears to be unaffected by changes in the biomineralization process that mediates the response to carbonate chemistry (Marchitto et al., 2018). Core-top values also have a better temperature correlation for Mg/Li ($R^2 = 0.90$) than Mg/Ca ($R^2 = 0.49$) (Bryan and Marchitto, 2008; Marchitto et al., 2018).

Here, we present the first temperature records from the South Atlantic based on the Mg/Li of *H. elegans*. The records span the last 0 to 30 kyr and 0 to 60 kyr, providing context for South Atlantic intermediate-depth and mid-depth temperature changes of the last deglaciation. We pair the Mg/Li-based temperature estimates with *Cibicidoides pachyderma* $\delta^{18}O$ to estimate the $\delta^{18}O$ of seawater ($\delta^{18}O_{sw}$; Lynch-Stieglitz et al., 1999; Marchitto et al., 2014), enabling us to identify the arrival of low-$\delta^{18}O_{sw}$ deglacial meltwater to the Brazil Margin sites. We use paired benthic foraminifera measurements of *H. elegans* cadmium/calcium ratios (Cd/Ca) and *C. pachyderma* $\delta^{13}C$ to estimate water mass nutrient properties and isolate the influence of air-sea gas exchange on $\delta^{13}C$ ($\delta^{13}C_{as}$; Lynch-Stieglitz and Fairbanks, 1994). As $\delta^{13}C_{as}$ is a nearly conservative water mass tracer, it allows us to assess whether temperature anomalies are associated with a particular water mass.

Downcore records were generated from three intermediate depth (~1.1-1.3 km) cores collected from two sites on the Brazil margin at ~27°S and one mid-depth (~1.9 km) core collected from ~ 23°S. Sediment core KNR159-5-90GGC (27°21.0'S, 46°37.79'W) and companion core KNR159-5-105JPC (27°21.0'S, 46°37.89'W) were collected from 1,108 m water depth, whereas sediment core KNR159-5-36GGC (27°15.16'S, 46°28.22'W) was collected slightly deeper, at 1,268 m water depth (Figure 1). Today these sites are located just below the low salinity core of Antarctic Intermediate Waters (AAIW) and within the mixing gradient with high salinity North Atlantic Deep Water (NADW; Supplementary Figure 1). Concentrations of PO_4 and Cd are elevated in AAIW relative to NADW (Middag et al., 2018; Figure 1), in part because CDW contributes nutrients to AAIW (Sarmiento et al., 2004), and in part because remineralization in the AAIW formation region increases the PO_4 values and reduces $\delta^{13}C$ values (Oppo et al., 2018). Mid-depth sediment core PC-CAM61 (22.52°S, 39.90°W) was collected from 1,890 m water depth, within the modern extent of NADW and

near its upper boundary with AAIW. As a result, it has lower PO_4 and Cd concentrations than the intermediate depth sites (Figure 1).

2. Methods

2.1 Age models

Age models for each of the Brazil margin cores were constructed using planktonic foraminifera radiocarbon dates (Supplementary Figure 2). Published ^{14}C ages for 90GGC (Lund et al., 2015) and 36GGC (Oppo et al., 2018; Sortor and Lund, 2011) were supplemented with 2 and 8 additional ^{14}C dates (Supplementary Figure 2), respectively. Unpublished planktonic ^{14}C dates were used to construct the age models for 105JPC and PC-CAM61 (Supplementary Figure 2). Following Lund et al. (2015), ^{14}C ages were corrected using a ΔR of 7 ±200 years (one sigma) to account for possible changes in the marine radiocarbon reservoir age through time. For 36GGC, the plateau-tuned age model from Balmer et al. (2016) was supplemented with eight new ^{14}C ages. However, the age model from Sortor and Lund (2011) was modified to utilize a ΔR of 7 ±200 years at core depths above the top of the Younger Dryas ^{14}C plateau; this avoids the application of Younger Dryas reservoir ages to Holocene samples. Final chronologies were constructed using the Bayesian age-modeling program Bacon (Blaauw and Christen, 2011).

2.2 Isotopic and trace element analysis

New benthic carbon and oxygen isotopic records were generated for 105JPC, and PC-CAM61 and the published record of 36GGC was supplemented with new data from ~22 to 30 kyr BP. New benthic isotope data were also generated for core 90GGC, as published glacial/late deglacial $\delta^{18}O$ values were higher than nearby, deeper core 36GGC (Curry and Oppo, 2005) inconsistent with their density contrast. The new data were generated on the benthic foraminiferal species *C. pachyderma* from 36GGC, 90GGC, and 105JPC, whereas *C. wuellerstorfi* were measured for PC-CAM61. Because *C. pachyderma* were generally absent

from the top 36.5 cm of 90GGC and the top 94.5 cm of 36GGC, *Cibicidoides sp.* were measured instead. New measurements were made using a Finnigan MAT253 mass spectrometer with a long-term laboratory precision of the NBS-19 carbonate standard of 1σ ±0.07‰ for $\delta^{18}O$ and ±0.02‰ for $\delta^{13}C$ (n>390.

Elemental ratios were determined using the benthic foraminiferal species *H. elegans* for 36GGC, 90GGC, and 105JPC. Samples of ~10 *H. elegans* from 90GGC and 105JPC were crushed, homogenized and split into replicates. For material-limited 90GGC and 105JPC samples <5 *H. elegans* were used. Elemental ratios were also determined using the benthic foraminiferal species *Uvigerina perigrina* and *C. wuellerstorfi* from PC-CAM61 and Mg/Ca based temperatures from those species were compared to the *H. elegans* Mg/Li-based temperature estimates from that core (Supplementary Figure 3). Each sample was reductively and oxidatively cleaned following Boyle and Keigwin (1985) as modified by Boyle and Rosenthal (1996). Analysis of 90GGC, 105JPC, and PC-CAM61 samples were carried out on a Thermo Scientific iCap Qc Inductively Coupled Plasma Mass Spectrometer (ICP-MS) at Woods Hole Oceanographic Institution. Consistency was monitored over the course of these analyses through repeated analysis of four standards with Mg/Ca ratios of 0.58, 1.21, 3.30, and 7.33 mmol/mol and Li/Ca ratios of 2.14, 13.46, 26.41, and 43.04 μmol/mol. The Mg/Ca long-term 1σ-precision of the standards was ±0.01 (1.8%), ±0.02 (1.4%), ±0.03 (0.8%), and ±0.12 (1.6%), respectively. The Li/Ca long-term 1σ-precision of the standards was ±0.05 (2.1%), ±0.18 (1.3%), ±0.44 (1.7%), and ±0.73 (1.7%), respectively. The Cd/Ca long term precision was ±0.003 (3.9%), ±0.033 (1.9%), ±0.033 (1.9%), and ±0.036 (1.9%) for four standards with Cd/Ca ratios of 0.071, 1.737, 1.802, and 1.884 μmol/mol, respectively. The long-term consistency for Mg/Li is ±0.007 (2.5%), ±0.002 (1.9%), ±0.002 (1.6%), ±0.003 (2.0%) for standards with Mg/Li ratios of 0.272, 0.090, 0.125, and 0.170, respectively.

Analysis of 36GGC was carried out on a Varian ICP 820MS at the Australian National University. Samples of ~1-6 *H. elegans* from 36GGC were crushed, homogenized and split into replicates. Comparison of data measured for samples of various sizes suggest relatively homogeneous Mg/Li ratios for *H. elegans* (Supplementary Figure 4). Elemental ratios were also determined using the benthic foraminiferal species *U. peregrina* and *C. pachyderma* from 36GGC and Mg/Ca-based temperatures from those species were compared to the *H. elegans* Mg/Li-based temperature estimates from that core (Supplementary Figure 5). Samples were reductively and oxidatively cleaned following Boyle and Keigwin (1985) as modified by Boyle and Rosenthal (1996). As the reductive cleaning step has been shown to selectively dissolve foraminiferal calcite (Yu and Elderfield, 2007), the reductive cleaning step was omitted for several replicates to test whether the Mg/Li ratios of oxidatively cleaned samples were reproduced. We found no significant differences in Mg/Li between samples cleaned with and without the reductive step (Supplementary Figure 4). The long-term consistency for Mg/Li is <~2% (Yu et al., 2005).

H. elegans has a glassy aragonitic test that has been suggested to be less prone to diagenetic overgrowths (Boyle et al., 1995). Ratios of Al/Ca, Mn/Ca, and Fe/Ca were used to monitor contamination and were generally negligible. However, samples with elevated Al/Ca, Mn/Ca and/or Fe/Ca ratios were excluded from the final results due to suspected contamination. Relatively young radiocarbon dates in the deglacial sections of several KNR159-5 cores, including 90GGC, suggest that the records from these cores may be influenced by deep burrowing, a hypothesis confirmed by Holocene-like planktonic $\delta^{18}O$ values in the deglacial section of a deeper core (Lund et al., 2015). However, because the planktonic-to-benthic ratio is as high as 3000 in the early Holocene, compared to ~ 250 in the deglacial and glacial sections, bioturbation had a much larger influence on the planktonic than benthic $\delta^{18}O$ record (Broecker et al., 1999; Lund et al., 2015). As only 1-6 *H. elegans*

are generally required for elemental analyses, one transported or mixed individual can impact the measured elemental ratio. To account for any mixing samples were measured in duplicate and triplicate whenever possible. Data points that were outliers in a set of 3 or more replicate analyses or data points that fell outside ±2σ of the mean for the core were excluded from our final interpretation of the data. These results may be influenced by bioturbation (marked as x's in Figures 2-4). Unfortunately, additional samples from PC-CAM-61 are not available, and we were not able to improve the resolution of records from that core.

2.3 Temperature estimation

Bottom water temperature (BWT) was estimated from *H. elegans* Mg/Li ratios by expanding upon the cold end of the core top calibration of Marchitto et al. (2018; Eq. 1) with four additional core top samples collected from <7°C and measured in triplicate (Eq. 2; Supplementary Fig. 3). The standard errors of temperature estimates are ±0.9°C at 0°C and ±1.1°C at 7°C, with a Mg/Li standard error of estimate of ±0.018 mol/mmol for Eq. 2. Despite only minor differences between the calibration of Ref. 20 (Eq. 1) and the calibration equation developed here (Eq. 2) the additional data points reduce the cold-end scatter and decrease the temperature estimate errors. Paired foraminiferal $\delta^{18}O$ values ($\delta^{18}O_{calcite}$) and Mg/Li temperature estimates were used to estimate the $\delta^{18}O$ composition of seawater ($\delta^{18}O_{SW}$) using the revised calibration of (Marchitto et al., 2014; Eq. 3) for *Cibicidoides* and *Planulina*. The *H. elegans*, *Cibicidoides,* and *U. peregrina.* Mg/Ca estimated temperatures are inconsistent with our *H. elegans* Mg/Li temperature estimates, highlighting the unreliability of benthic Mg/Ca-based temperature estimates (Supplementary Figure 5).

$$Mg/Li = 0.150 \pm 0.012 + 0.0209 \pm 0.0027*T - 0.0002 \pm 0.0001*T^2 \qquad R^2 = 0.95$$

(Eq. 1)

$$Mg/Li = 0.160 \pm 0.010 + 0.0211 \pm 0.0023*T - 0.0003 \pm 0.0001*T^2 \qquad R^2 = 0.96$$

(Eq. 2)

$(\delta^{18}O_{calcite} - \delta^{18}O_{SW} + 0.27) = -0.245 \pm 0.005 * T + 0.0011 \pm 0.0002 * T^2 + 3.58 \pm 0.02$ (Eq. 3)

2.4 Isolation of the carbon isotopic air-sea signature

The $\delta^{13}C$ value of a water mass reflects both biological fractionation during photosynthesis and respiration, and physical fractionation during air-sea gas exchange, which is influenced by the residence time of waters at the surface and the extent of temperature-dependent equilibration of surface waters with the atmosphere (Broecker and Peng, 1982; Charles et al., 1993; Inoue and Sugimura, 1985; Lynch-Stieglitz et al., 1995). The cadmium composition of seawater is positively correlated with the nutrient phosphate (Boyle, 1988), although nutrient-depleted waters are characterized by lower Cd/phosphate ratios than nutrient-rich waters (Middag et al., 2018; Xie et al., 2015). The aragonitic foraminifera *H. elegans* records the cadmium concentration of seawater (Cd_W) with little depth dependence (Boyle et al., 1995). Cd_W values were estimated from *H. elegans* Cd/Ca using the Cd partition coefficient D=1 from Boyle (1992). Following Lynch-Stieglitz and Fairbanks (1994), we used paired Cd/Ca and $\delta^{13}C$ measurements to isolate the air-sea signature of $\delta^{13}C$ ($\delta^{13}C_{as}$; Figures 3 and 4). We provide new equations for estimating $\delta^{13}C_{as}$ using the relationship between $\delta^{13}C$ and PO_4^{3-} from Eide et al. (2017; Eq. 3), slightly modified from Broecker and Maier-Reimer (1992):

$\delta^{13}C_{bio} = 2.8 - 1.1*PO_4$ (Eq. 3)

and the relationships between Cd and PO_4 observed in Atlantic transects of Cd and PO_4 for a low-nutrient (PO_4^{3-}<1.3 µmol/kg), North Atlantic endmember (Eq. 4) and a high-nutrient (PO_4^{3-}>1.3 µmol/kg), Southern Ocean endmember (Eq. 5), rather than the high and low nutrient endmembers estimated using the global compilation from Boyle (1988).

$Cd_W = 0.287 *PO_4^{3-} - 0.066$ (Eq. 4)

$Cd_W = 0.463 *PO_4^{3-} - 0.303$ (Eq. 5)

The resulting equations for $\delta^{13}C_{as}$ for PO_4^{3-}<1.3 µmol/kg (Eq. 6) and PO_4^{3-}>1.3 µmol/kg (Eq. 7) are:

$$\delta^{13}C_{as} = \delta^{13}C_{measured} + 3.83*Cd_W - 2.55 \quad \text{(Eq. 6)}$$

$$\delta^{13}C_{as} = \delta^{13}C_{measured} + 2.38*Cd_W - 2.08 \quad \text{(Eq. 7)}$$

Following Lynch-Stieglitz and Fairbanks (1994), glacial $\delta^{13}C_{as}$ estimates take into consideration 2‰ higher organic matter $\delta^{13}C$, 0.3‰ lower mean ocean $\delta^{13}C$, and a ~4% increase in total inorganic carbon during the last glacial period for both the low-nutrient (PO_4^{3-}<1.3 µmol/kg; (Eq. 8) and high-nutrient (PO_4^{3-}>1.3 µmol/kg; Eq. 9) glacial endmembers.

$$\delta^{13}C_{as} = \delta^{13}C_{measured} + 3.31*Cd_W - 1.98 \quad \text{(Eq. 8)}$$

$$\delta^{13}C_{as} = \delta^{13}C_{measured} + 2.05*Cd_W - 1.58 \quad \text{(Eq. 9)}$$

Plots of Cd_W vs $\delta^{13}C$ indicate that glacial PO_4^{3-} was likely higher than 1.3 µmol kg^{-1} at our AAIW site (Figure 5). However, the evolution from glacial to Holocene $\delta^{13}C_{as}$ is uncertain (Supplementary Figure 7), as the timing of changes in the $\delta^{13}C$ of marine organic matter and the ocean's dissolved inorganic carbon inventory are not well constrained.

If a $\delta^{13}C$ change is caused by a change in the accumulation of respired material, a commensurate change in nutrients (or estimated seawater Cd_W) should be observed, resulting in no change in $\delta^{13}C_{as}$. A $\delta^{13}C$ change without an accompanying change in estimated Cd_W would imply that the $\delta^{13}C$ change was not associated with a change in respired nutrients, but rather a change in the air-sea exchange signature of a source water to the site. Contrarily, a change in Cd_W without an accompanying change in $\delta^{13}C$ implies that the change in Cd_W was compensated for by a change in $\delta^{13}C_{as}$.

3. Results

3.1 South Atlantic subsurface temperature variability

Our new *H. elegans* Mg/Li-based temperature estimates reveal that temperatures between 1.1 and 1.9 km decreased gradually through Marine Isotope Stage (MIS) 3 (59.4-27.8 kyr BP) into MIS 2 (27.8-11.7 kyr BP; Figure 2b; Supplementary Figure 6), likely reflecting global-scale cooling. Notably, our temperature reconstructions reveal that western South Atlantic waters between 1.1 and 1.9 km warmed by ~2.5-3.0 °C from the Last Glacial Maximum (LGM, 17.5-23.3 kyr BP) to the Holocene (Figure 2b). Warming began at ~17.5 kyr BP, approximately coeval with the onset of HS1 at the two deeper sites (1.3 and 1.9 km), and perhaps as late as ~16.3 kyr BP at ~1.1 km. By the middle of HS1, these water depths were roughly isothermal, with at most a small gradient between PC-CAM61 (1.9 km) and the shallower sites. Strikingly, the warming was sustained through HS1 and continued into the BA, although at a lower rate (Figure 2b). Most of the warming associated with HS1 and the warming during HS1 was greater than at any other time during the last ~60 kyr (Figure 4). Earlier Heinrich events are not consistently associated with warming, despite evidence for AMOC decline (Lynch-Stieglitz et al., 2014).

At ~20 kyr BP, global ice volume began to decrease, the mean ocean to freshen, and the mean ocean seawater oxygen isotope value ($\delta^{18}O_{sw}$) to decrease (Figure 2c; Clark et al., 2009). Our sites document similar glacial-Holocene $\delta^{18}O_{sw}$ differences as the mean ocean (Figure 2c), with possible differences in $\delta^{18}O_{sw}$ evolution between PC-CAM61 and the shallower sites. Of note, $\delta^{18}O_{sw}$ recorded at intermediate depths did not begin to decrease until the end of HS1 or even later, lagging the mean ocean decrease by at least 5000 years, indicating a delay of deglacial meltwater to the site. Although gaps in the PC-CAM61 records preclude identifying the timing of the onset of the deglacial $\delta^{18}O_{sw}$ decrease, by late HS1

values had decreased as much as the mean ocean, suggesting an earlier arrival of deglacial freshwater than at shallower sites.

3.2 South Atlantic water mass properties

Paired Cd_W and $\delta^{13}C$ measurements allow us to place the warming documented at our sites from ~1.1-1.9 km water depth into the larger context of changes in water mass mixing and circulation. For most of the last 60,000 years, when we have data from both an AAIW-depth site (90GGC/105JPC, ~1.1 km) and the site within glacial NADW (PC-CAM-61; ~1.9 km), $\delta^{13}C$ was lower at the shallower site, consistent with AAIW overlying NADW as in the modern and glacial oceans (Curry and Oppo, 2005; Oppo et al., 2018; Figures 3-5). The Cd_W estimates from the mid-depth site at ~35 kyr BP are lower than coeval AAIW Cd_W estimates, consistent with the water mass geometry inferred from $\delta^{13}C$ (Figure 5). At about 28 kyr BP, AAIW Cd_W (and $\delta^{13}C_{as}$) decreased, resulting in the near-disappearance of the Cd_W gradient between the shallow and mid-depth sites, while the $\delta^{13}C$ gradient remained and a new $\delta^{13}C_{as}$ gradient was established (Figure 3). AAIW Cd_W values remained low until ~14.0 kyr BP despite an earlier $\delta^{13}C_{as}$ increase at ~16.5 kyr BP (Figure 3). The reason why AAIW Cd_W (and $\delta^{13}C_{as}$) decreased at this time (~MIS2-MIS3 transition) and remained low until ~14.0 kyr BP is unclear, but a connection to southern hemisphere processes is likely, as Antarctica also experienced the coldest temperatures (Figure 2a) and greatest ice volume (Clark et al., 2009; Figure 2c) of the last the last 60,000 years (Supplementary Figure 6) during this same interval. The $\delta^{13}C$ of AAIW decreased at ~24 kyr BP (~HS2), resulting in South Atlantic water mass properties that remained approximate constant until the end of the LGM.

Estimated Cd_W values were generally similar between ~1.1 and 1.9 km during the LGM, whereas $\delta^{13}C$ exhibited a strong gradient, with highest $\delta^{13}C$ at the mid-depth site (~1.9 km), lowest at the intermediate-depth sites (~1.1km) and that of the 1.3 km site falling in between (Figure 3), similar to the modern distribution of $\delta^{13}C$ in the South Atlantic

(Supplementary Figure 8). As $\delta^{13}C_{as}$ is quasi-conservative, higher values at ~1.9 km than at the shallower sites indicates that the cores were situated in different water masses during the LGM. Specifically, our results suggest that like today, the shallower sites were within (glacial) AAIW and the mid depth site within (glacial) NADW.

The $\delta^{13}C$ values of intermediate waters increased abruptly early in HS1, with little change in estimated Cd_W (Figure 3). Subsequently, estimated Cd_W of AAIW increased from late HS1/early BA through the BA (Figure 3). Finally, $\delta^{13}C$ gradually increased within the Holocene, with little change in Cd_W. This three-step deglacial evolution of AAIW properties is highlighted in Figure 4. $\delta^{13}C$ values decreased at 1.9 km during HS1 and returned to glacial-like values during the BA (Figure 3), consistent with previous evidence of a deglacial $\delta^{13}C$ minimum in the mid-depth South Atlantic (Tessin and Lund, 2013).

4. Discussion

Comparison of our downcore records to LGM and Holocene water mass properties provides insight into possible reasons why glacial properties of AAIW were so different from modern (Figure 5). During the LGM, Southern and Pacific Ocean end-members had lower Cd_w, $\delta^{13}C$, and $\delta^{13}C_{as}$ values than during the Holocene (Boyle, 1992; Eide et al., 2017; Lynch-Stieglitz et al., 1996; Marchitto and Broecker, 2006; Middag et al., 2018; Oppo and Horowitz, 2000) (Figure 5). In contrast, glacial NADW shows little to no difference in Cd_w, and slightly higher $\delta^{13}C$ and $\delta^{13}C_{as}$ values relative to the Holocene (Boyle, 1992; Eide et al., 2017; Lynch-Stieglitz et al., 1996; Marchitto and Broecker, 2006; Middag et al., 2018; Oppo et al., 2018). Whereas $\delta^{13}C_{as}$ was higher in the Southern Ocean than North Atlantic during the Holocene (and in the modern), during the LGM, $\delta^{13}C_{as}$ was higher in the North Atlantic (Oppo et al., 2018) (Figure 5). These changes suggest that glacial North Atlantic surface source waters were better equilibrated with the atmosphere, perhaps due to colder temperatures and in turn a stronger fractionation during air-sea exchange there, with the

opposite being the case for southern sourced waters, perhaps because of greater sea-ice extent.

Glacial Cd_w and $\delta^{13}C$ estimates in the South Atlantic at modern AAIW depths (90GGC, 105JPC) are both lower than Holocene estimates (Figures 3-5), and this decoupling between nutrients and $\delta^{13}C$ gives rise to the low glacial $\delta^{13}C_{as}$ values. The Cd_w versus $\delta^{13}C$ cross-plots (Figure 5) suggest that glacial CDW $\delta^{13}C$ and Cd_w values were much lower than Holocene values. They also show AAIW falling along a mixing line that connects CDW with NADW, similar to the modern ocean. Thus, even with a similar contribution of CDW to AAIW as in the Holocene, glacial AAIW properties could reflect changes in the CDW endmember.

Several related changes resulting from an AMOC decline would be expected to lead to a $\delta^{13}C$ increase at our AAIW sites, as observed in HS1. For example, model simulations suggest an AMOC decline would result in less remineralized components in CDW (Schmittner and Lund, 2015), which could influence the properties of AAIW. The same simulations suggest an AMOC decline would result in less remineralization within AAIW as well as a reduced return flow of low-$\delta^{13}C$ intermediate-depth waters from the Indian Ocean. An AMOC decline would cause a deepening of the thermocline (Hain et al., 2014), as observed in model simulations at the latitude of our sites (Zhang et al., 2017), which would also increase the $\delta^{13}C$. However, all these mechanisms would result in lower nutrients, and presumably lower Cd_W, which is not observed. The small Cd_W decrease compared to the large $\delta^{13}C$ increase for all these mechanisms suggests that these processes were not the only or main cause of the $\delta^{13}C$ decrease or that a more nutrient-rich water mass with higher $\delta^{13}C_{as}$ contributed to AAIW or to the water-mass mixture at our core sites, compensating for some expected Cd_W decrease. For example, greater upwelling of deep water, perhaps due to a poleward shift in the southern hemisphere westerlies (e.g. Menviel et al., 2018) might have

increased nutrients and decreased $\delta^{13}C$ of waters contributing to AAIW. However, outgassing of low-$\delta^{13}C$ CO_2 would decouple $\delta^{13}C$ from nutrients, leading to higher $\delta^{13}C_{as}$ in this hypothesized AAIW source water. The atmospheric CO_2 increase (Monnin et al., 2001) and $\delta^{13}C$ decrease (Bauska et al., 2016) approximately synchronously with HS1also suggests that some portion of the mean ocean $\delta^{13}C$ increase 0.3±0.2‰; Gebbie et al., 2015) occurred at this time, and regardless of the exact mechanism, likely contributed to the observed HS1 decoupling between $\delta^{13}C$ and CdW (Supplementary Figure 7). Finally, as noted, there are systematic differences in the Cd/PO_4 ratio among different water masses (Middag et al., 2018). While we cannot constrain potential decoupling between Cd and phosphate in the past, the systematic differences in the modern ocean, with higher Cd/phosphate ratios in nutrient-rich than nutrient-poor waters, are in the wrong direction to explain the small Cd_W decrease when $\delta^{13}C$ increases, if $\delta^{13}C$ increase was due to a nutrient increase.

Changes in $\delta^{13}C$ and estimated Cd_W at the mid-depth core reinforce previous evidence of a reduced AMOC during HS1. Our estimate of HS1 Cd_W hints at an increase in mid-depth nutrients during HS1, providing evidence that $\delta^{13}C$ and carbonate ion decreases in mid-depth South Atlantic waters (Lacerra et al., 2017; Lund et al., 2015) were associated with enhanced accumulation of respired organic material, likely in association with a weaker AMOC. Likewise, the reduced vertical property gradients are also characteristic of an AMOC decline (Schmittner and Lund, 2015).

Cd_W increased in AAIW near the onset of the BA, reflecting AMOC reinvigoration and the associated increase in Indian Ocean water supply to Atlantic AAIW, shoaling of the thermocline and AAIW, and higher nutrients in CDW. Deglacial records of water mass radiocarbon content and $\delta^{11}B$-estimated pH from the Southern Ocean suggest enhanced vertical exchange at this time (Burke and Robinson, 2012; Martínez-Botí et al., 2015; Rae et al., 2018), which may have contributed to higher nutrient content in AAIW. However, the

$\delta^{13}C$ of AAIW did not decrease (Figures 3-5), suggesting that the continued trend towards enhanced Holocene air-sea gas exchange compensated for any nutrient-driven $\delta^{13}C$ decrease. The $\delta^{13}C$ and Cd_W of the mid-depth site also increased and decreased respectively, signaling a decrease in remineralized components in association with the BA AMOC strengthening. The $\delta^{13}C$ of AAIW continued to increase throughout the Holocene without significant changes in its Cd_W. While some of the early Holocene $\delta^{13}C$ rise likely reflects the increasing $\delta^{13}C$ of the atmospheric (Lynch-Stieglitz et al., 2019), the magnitude of the increase exceeds that of the atmosphere and likely reflects a trend of enhanced air-sea equilibration in AAIW source waters. Some component of the Holocene $\delta^{13}C$ rise might also reflect continuing mean ocean $\delta^{13}C$ increase.

The $\delta^{13}C$ and Cd_w evidence that the intermediate and mid-depth sites were respectively situated in AAIW and NADW during glacial times, as they are today, indicates that deglacial warming was not uniquely associated with either glacial water mass. Moreover, as shallow North Atlantic waters were likely characterized by low $\delta^{18}O_{sw}$ (Zhang et al., 2017), the early arrival of low $\delta^{18}O_{sw}$ at the mid-depth site suggests a northern origin of warming. On the other hand, the arrival of low $\delta^{18}O_{sw}$ at AAIW depths after HS1 (Figure 2) strongly suggests that southward advection of heat anomalies within NADW did not contribute significantly to early deglacial warming at the shallower cores sites. Our data further reveal that warming continued, although at a lower rate, after HS1 and into the late BA. As cooling is expected in response to an AMOC recovery (Figures 6 and 7; Liu et al., 2009), this finding suggests an additional forcing mechanism was responsible for the absence of cooling and continued subsurface warming. In fact, AMOC variability was not the only potential deglacial driver of subsurface temperature variability, as atmospheric CO_2 was rising (Monnin et al., 2001) and ice sheets were retreating (Clark et al., 2009).

Consistent with our observations of warming at both NADW and AAIW depths, during HS1, model simulations suggest Atlantic-wide thermal anomalies associated with AMOC disruption (Galbraith et al., 2016; Liu et al., 2009; Pedro et al., 2018; Zhang et al., 2017). To evaluate the relative contribution of various potential forcings to subsurface warming even after the BA AMOC recovery, we compare transient simulations using the National Center for Atmospheric Research Community Climate System Model version 3 (NCAR CCSM3; Liu et al., 2009; Pedro et al., 2018; Zhang et al., 2017) forced by individual deglacial forcings (orbital forcing (ORB), melt water forcing (MWF), ice sheet forcing (ICE), and greenhouse gas forcing (GHG)) to the simulation with the full suite of deglacial forcings (TRACE).

Consistent with previous results for HS1, the TRACE simulation (Figures 5a & 6), predicts the greatest subsurface warming in the subpolar North Atlantic, where deep convection and exchange with the overlying cold atmosphere are reduced, and in the South Atlantic thermocline where anomalous heat builds up due to reduced cross-equatorial volume transport (Galbraith et al., 2016; Liu et al., 2009; Pedro et al., 2018; Zhang et al., 2017). A comparison of the TRACE and single forcing runs confirms that meltwater forcing dominates this response, consistent with the hypothesis that a weakened AMOC caused basin-wide subsurface temperature responses during HS1.

The simulation including all forcings (TRACE) predicts zonally averaged HS1 warming of 2-3°C above 1.0 km in the South Atlantic (Liu et al., 2009; Pedro et al., 2018; Zhang et al., 2017; Figure 5a), similar to a simulation using the coupled ocean-atmosphere model CM2Mc (Galbraith et al., 2016). The simulation confirms that HS1 warming at these shallower core sites was likely due to heat accumulation resulting from reduced northward heat transport and a relatively deep extension of the South Atlantic thermocline anomaly (Galbraith et al., 2016; Liu et al., 2009; Pedro et al., 2018; Zhang et al., 2017). Model

simulations suggest that during AMOC weakening, warming at the depths of our shallow cores is enhanced by reduced upwelling and thermocline deepening (Galbraith et al., 2016; Liu et al., 2009; Pedro et al., 2018; Zhang et al., 2017), potentially consistent with the increase in the $\delta^{13}C$ of AAIW, as discussed above.

Our records document HS1 warming of similar magnitude (2.5-3.0 °C) at our mid-depth site, where zonally-averaged simulated warming is only ~0.5-1.5°C (Galbraith et al., 2016; Liu et al., 2009; Pedro et al., 2018; Zhang et al., 2017). Within NADW, more warming is expected along the deep western boundary compared to the zonal mean (Figure 5f & g), as North Atlantic shallow subsurface thermal anomalies are advected in the deep western boundary current. Given a relatively shallow glacial NADW, southward flow occurred at mid water depths, where the PC-CAM-61 site is situated. HS1 warming at the core's grid cell was ~2°C (Supplementary Figure 9), similar to our Mg/Li-based estimate.

Antarctic ice core noble gases suggest a magnitude and onset of deglacial warming for the mean ocean (Bereiter et al., 2018) similar to those we reconstruct at intermediate and mid depths of the South Atlantic (Supplementary Figure 10). This finding is consistent with evidence that ocean warming during AMOC collapse is initially concentrated in the Atlantic above 2 km (Figure 5a), before propagating to the global ocean and eventually contributing to the warming of the high-latitude Southern Ocean (Galbraith et al., 2016; Pedro et al., 2018).

Upon AMOC resumption at the onset of the BA, models predict a brief cooling in the South Atlantic thermocline as trapped heat is rapidly advected northward in the upper limb of the AMOC (e.g. Figure 6b; Galbraith et al., 2016; Pedro et al., 2018). We do not, however, document cooling between 1.1 and 1.3 km during the BA AMOC resumption. The simulations suggest that ice sheet decay contributed to warming late in the deglaciation (Figures 6 & 7), as orographic effects of a smaller ice sheet resulted in poleward migration of the westerly jet, allowing the expansion of sea ice in the Labrador Sea, reducing convection,

and curtailing heat loss to the atmosphere (Zhu et al., 2014). This finding leads us to hypothesize that ice volume forcing began to warm the South Atlantic earlier than predicted by the simulations, before AMOC recovery, offsetting cooling due to the AMOC recovery at our sites, and instead resulting in the observed (Figure 2) sustained modest warming in the early deglacial South Atlantic subsurface during the BA.

There was no discernable warming during the Younger Dryas, another period also associated with evidence of AMOC weakening. Less extensive ice sheets during the Younger Dryas, a different routing of freshwater, and/or an already warm subsurface South Atlantic may have been responsible for maintaining the warm temperatures of HS1. The absence of detectable South Atlantic subsurface warming during the Younger Dryas, when both CO_2 and Southern Hemisphere temperatures increased significantly (Monnin et al., 2001; Parrenin et al., 2013; Figures 2 & 3), suggests that intermediate depth warming associated with CO_2-driven temperature increases of endmember surface waters (Menviel et al., 2015) did not contribute significantly to the observed deglacial warming at our sites, consistent with our model evidence that it played a minor role (Figures 5 and 6). Similarly, the lack of a consistent warming during earlier MIS3 Heinrich events (Supplementary Figure 6) suggests smaller AMOC reductions, or that background climate or oceanic conditions were not favorable for warming in the South Atlantic.

5. Conclusions

Unlike Cd_W, $\delta^{13}C$, and $\delta^{13}C_{as}$, which indicate changes in chemical stratification associated with deglacial AMOC variability, Mg/Li-based subsurface temperatures exhibit similar trends and amplitudes over the depth range of our cores (1000-2000 m). We have used independent information from these data, $\delta^{18}O_{sw}$ estimates, and transient model simulations to identify and confirm the role of several forcings and their interactions on

subsurface Atlantic temperature change. Our results provide the first evidence of the link between large-scale heat distribution and severe AMOC collapse predicted by models (Galbraith et al., 2016; Liu et al., 2009; Marcott et al., 2011; Pedro et al., 2018; Zhang et al., 2017). Furthermore, we show that subsurface South Atlantic warming, while not restricted to a single water mass, was driven primarily by AMOC collapse during HS1. Data and model simulations each provide strong evidence that during HS1, heat trapping warmed AAIW and the advection of a North Atlantic warm anomaly warmed NADW in the South Atlantic. The model simulations identify ice sheet retreat as a significant forcing that extended subsurface Atlantic warming past HS1 and through the BA, as observed. Both data and model simulations imply that rising CO_2 did not significantly influence South Atlantic temperatures between 1 and 2 km, with the model simulations suggesting the contribution of CO_2 forcing to subsurface warming was strongest in the North Atlantic above 2km.

Acknowledgements

We thank H. Abrams, G. Swarr, and J. Watson for technical assistance. This work was funded by United States National Science Foundation grant OCE15-558341, the Investment in Science Fund at the Woods Hole Oceanographic Institution, and an Australian Research Council Future Fellowship (FT140100993). The data are included in the Supporting Information and are available at https://www.ncdc.noaa.gov/paleo/study/26530.

Author Contributions

NEU performed the research and wrote the manuscript with DWO, with significant contributions from ZL. NEU generated the 90GGC and 105JPC elemental data; PC, ZDJ, and NEU generated the 36GGC elemental data; KRP generated the new benthic isotope data.; ZL and MY analyzed the model output. All coauthors approved submission.

Competing Interests

The authors declare no competing interests

References

Balmer, S., Sarnthein, M., Mudelsee, M., & Grootes, P. M. (2016). Refined modeling and ^{14}C plateau tuning reveal consistent patterns of glacial and deglacial ^{14}C reservoir ages of surface waters in low-latitude Atlantic. *Paleoceanography*, *31*(8), 1030–1040. https://doi.org/10.1002/2016PA002953

Bauska, T. K., Baggenstos, D., Brook, E. J., Mix, A. C., Marcott, S. A., Petrenko, V. V., et al. (2016). Carbon isotopes characterize rapid changes in atmospheric carbon dioxide during the last deglaciation. *Proceedings of the National Academy of Sciences*, *113*(13), 3465–3470. https://doi.org/10.1073/pnas.1513868113

Bereiter, B., Eggleston, S., Schmitt, J., Nehrbass-Ahles, C., Stocker, T. F., Fischer, H., et al. (2015). Revision of the EPICA Dome C CO_2 record from 800 to 600 kyr before present: Analytical bias in the EDC CO_2 record. *Geophysical Research Letters*, *42*(2), 542–549. https://doi.org/10.1002/2014GL061957

Bereiter, B., Shackleton, S., Baggenstos, D., Kawamura, K., & Severinghaus, J. (2018). Mean global ocean temperatures during the last glacial transition. *Nature*, *553*(7686), 39–44. https://doi.org/10.1038/nature25152

Blaauw, M., & Christen, J. A. (2011). Flexible paleoclimate age-depth models using an autoregressive gamma process. *Bayesian Analysis*, *6*(3), 457–474. https://doi.org/10.1214/11-BA618

Bond, G., Heinrich, H., Broecker, W., Labeyrie, L., McManus, J., Andrews, J., et al. (1992). Evidence for massive discharges of icebergs into the North Atlantic ocean during the last glacial period. *Nature*, *360*, 245.

Boyle, E. A. (1988). Cadmium: Chemical tracer of deepwater paleoceanography. *Paleoceanography*, *3*(4), 471–489. https://doi.org/10.1029/PA003i004p00471

Boyle, E A. (1992). Cadmium and $\delta^{13}C$ Paleochemical Ocean Distributions During the Stage 2 Glacial Maximum. *Annual Review of Earth and Planetary Sciences*, *20*(1), 245–287. https://doi.org/10.1146/annurev.ea.20.050192.001333

Boyle, E.A., & Keigwin, L. D. (1985). Comparison of Atlantic and Pacific paleochemical records for the last 215,000 years: changes in deep ocean circulation and chemical inventories. *Earth and Planetary Science Letters*, *76*(1–2), 135–150. https://doi.org/10.1016/0012-821X(85)90154-2

Boyle, E.A., & Rosenthal, Y. (1996). Chemical hydrography of the South Atlantic during the last glacial maximum: Cd vs. d13C. In *The South Atlantic: Present and Past Circulation* (pp. 423–443). Springer-Verlag.

Boyle, Edward A., Labeyrie, L., & Duplessly, J.-C. (1995). Calcitic foraminiferal data confirmed by cadmium in aragonitic *Hoeglundina*: Application to the Last Glacial Maximum in the northern Indian Ocean. *Paleoceanography*, *10*(5), 881–900. https://doi.org/10.1029/95PA01625

Broecker, W. S., & Maier-Reimer, E. (1992). The influence of air and sea exchange on the carbon isotope distribution in the sea. *Global Biogeochemical Cycles*, *6*(3), 315–320. https://doi.org/10.1029/92GB01672

Broecker, W. S., & Peng, T.-H. (1982). *Tracers in the Sea*. Palisades, New York: Lamont-Doherty Geological Observatory, Columbia University.

Broecker, W. S., Peteet, D. M., & Rind, D. (1985). Does the ocean–atmosphere system have more than one stable mode of operation? *Nature*, *315*, 21.

Broecker, W. S., Bond, G., Klas, M., Bonani, G., & Wolfli, W. (1990). A salt oscillator in the glacial Atlantic? 1. The concept. *Paleoceanography*, *5*(4), 469–477. https://doi.org/10.1029/PA005i004p00469

Broecker, W., Matsumoto, K., Clark, E., Hajdas, I., & Bonani, G. (1999). Radiocarbon age differences between coexisting foraminiferal species. *Paleoceanography*, *14*(4), 431–436. https://doi.org/10.1029/1999PA900019

Bryan, S. P., & Marchitto, T. M. (2008). Mg/Ca-temperature proxy in benthic foraminifera: New calibrations from the Florida Straits and a hypothesis regarding Mg/Li. *Paleoceanography*, *23*(2). https://doi.org/10.1029/2007PA001553

Burke, A., & Robinson, L. F. (2012). The Southern Ocean's Role in Carbon Exchange During the Last Deglaciation. *Science*, *335*(6068), 557–561. https://doi.org/10.1126/science.1208163

Came, R. E., Oppo, D. W., Curry, W. B., & Lynch-Stieglitz, J. (2008). Deglacial variability in the surface return flow of the Atlantic meridional overturning circulation. *Paleoceanography*, *23*(1). https://doi.org/10.1029/2007PA001450

Charles, C. D., Wright, J. D., & Fairbanks, R. G. (1993). Thermodynamic influences on the marine carbon isotope record. *Paleoceanography*, *8*(6), 691–697. https://doi.org/10.1029/93PA01803

Clark, P. U., Dyke, A. S., Shakun, J. D., Carlson, A. E., Clark, J., Wohlfarth, B., et al. (2009). The Last Glacial Maximum. *Science*, *325*(5941), 710–714. https://doi.org/10.1126/science.1172873

Clark, Peter U., Pisias, N. G., Stocker, T. F., & Weaver, A. J. (2002). The role of the thermohaline circulation in abrupt climate change. *Nature*, *415*, 863.

Cuffey, K. M., Clow, G. D., Steig, E. J., Buizert, C., Fudge, T. J., Koutnik, M., et al. (2016). Deglacial temperature history of West Antarctica. *Proceedings of the National Academy of Sciences*, *113*(50), 14249–14254. https://doi.org/10.1073/pnas.1609132113

Curry, W. B., & Oppo, D. W. (2005). Glacial water mass geometry and the distribution of $\delta^{13}C$ of ΣCO_2 in the western Atlantic Ocean. *Paleoceanography*, *20*(1). https://doi.org/10.1029/2004PA001021

Eide, M., Olsen, A., Ninnemann, U. S., & Johannessen, T. (2017). A global ocean climatology of preindustrial and modern ocean $\delta^{13}C$. *Global Biogeochemical Cycles*, *31*(3), 515–534. https://doi.org/10.1002/2016GB005473

Elderfield, H., Yu, J., Anand, P., Kiefer, T., & Nyland, B. (2006). Calibrations for benthic foraminiferal Mg/Ca paleothermometry and the carbonate ion hypothesis. *Earth and Planetary Science Letters*, *250*(3–4), 633–649. https://doi.org/10.1016/j.epsl.2006.07.041

Elderfield, H., Greaves, M., Barker, S., Hall, I. R., Tripati, A., Ferretti, P., et al. (2010). A record of bottom water temperature and seawater $\delta^{18}O$ for the Southern Ocean over the past 440kyr based on Mg/Ca of benthic foraminiferal Uvigerina spp. *Quaternary Science Reviews*, *29*(1–2), 160–169. https://doi.org/10.1016/j.quascirev.2009.07.013

François, R., Altabet, M. A., Yu, E.-F., Sigman, D. M., Bacon, M. P., Frank, M., et al. (1997). Contribution of Southern Ocean surface-water stratification to low atmospheric CO_2 concentrations during the last glacial period. *Nature*, *389*, 929–935. https://doi.org/10.1038/40073

Galbraith, E. D., Merlis, T. M., & Palter, J. B. (2016). Destabilization of glacial climate by the radiative impact of Atlantic Meridional Overturning Circulation disruptions. *Geophysical Research Letters*, *43*(15), 8214–8221. https://doi.org/10.1002/2016GL069846

Gebbie, G., Peterson, C. D., Lisiecki, L. E., & Spero, H. J. (2015). Global-mean marine $\delta^{13}C$ and its uncertainty in a glacial state estimate. *Quaternary Science Reviews*, *125*, 144–159. https://doi.org/10.1016/j.quascirev.2015.08.010

Hain, M. P., Sigman, D. M., & Haug, G. H. (2014). Distinct roles of the Southern Ocean and North Atlantic in the deglacial atmospheric radiocarbon decline. *Earth and Planetary Science Letters*, *394*, 198–208. https://doi.org/10.1016/j.epsl.2014.03.020

Inoue, H., & Sugimura, Y. (1985). Carbon isotopic fractionation during the CO2 exchange process between air and sea water under equilibrium and kinetic conditions. *Geochimica et Cosmochimica Acta*, *49*(11), 2453–2460. https://doi.org/10.1016/0016-7037(85)90245-5

John, S. G., Helgoe, J., & Townsend, E. (2018). Biogeochemical cycling of Zn and Cd and their stable isotopes in the Eastern Tropical South Pacific. *Marine Chemistry*, *201*, 256–262. https://doi.org/10.1016/j.marchem.2017.06.001

Jouzel, J., Masson-Delmotte, V., Cattani, O., Dreyfus, G., Falourd, S., Hoffmann, G., et al. (2007). Orbital and Millennial Antarctic Climate Variability over the Past 800,000 Years. *Science*, *317*(5839), 793–796. https://doi.org/10.1126/science.1141038

Key, R. M., Kozyr, A., Sabine, C. L., Lee, K., Wanninkhof, R., Bullister, J. L., et al. (2004). A global ocean carbon climatology: Results from Global Data Analysis Project (GLODAP). *Global Biogeochemical Cycles*, *18*(4). https://doi.org/10.1029/2004GB002247

Lacerra, M., Lund, D., Yu, J., & Schmittner, A. (2017). Carbon storage in the mid-depth Atlantic during millennial-scale climate events: Mid-depth Atlantic Carbon Storage. *Paleoceanography*, *32*(8), 780–795. https://doi.org/10.1002/2016PA003081

Liu, Z., Otto-Bliesner, B. L., He, F., Brady, E. C., Tomas, R., Clark, P. U., et al. (2009). Transient Simulation of Last Deglaciation with a New Mechanism for Bolling-Allerod Warming. *Science*, *325*(5938), 310–314. https://doi.org/10.1126/science.1171041

Lund, D. C., Tessin, A. C., Hoffman, J. L., & Schmittner, A. (2015). Southwest Atlantic water mass evolution during the last deglaciation. *Paleoceanography*, *30*(5), 477–494. https://doi.org/10.1002/2014PA002657

Lynch-Stieglitz, J. (2017). The Atlantic Meridional Overturning Circulation and Abrupt Climate Change. *Annual Review of Marine Science*, *9*(1), 83–104. https://doi.org/10.1146/annurev-marine-010816-060415

Lynch-Stieglitz, J., & Fairbanks, R. G. (1994). A conservative tracer for glacial ocean circulation from carbon isotope and palaeo-nutrient measurements in benthic foraminifera. *Nature*, *369*(6478), 308–310. https://doi.org/10.1038/369308a0

Lynch-Stieglitz, J., Stocker, T. F., Broecker, W. S., & Fairbanks, R. G. (1995). The influence of air-sea exchange on the isotopic composition of oceanic carbon: Observations and modeling. *Global Biogeochemical Cycles*, *9*(4), 653–665. https://doi.org/10.1029/95GB02574

Lynch-Stieglitz, J., van Geen, A., & Fairbanks, R. G. (1996). Interocean exchange of glacial North Atlantic Intermediate Water: Evidence from subantarctic Cd/Ca and carbon isotope measurements. *Paleoceanography*, *11*(2), 191–201. https://doi.org/10.1029/95PA03772

Lynch-Stieglitz, J., Curry, W. B., & Slowey, N. (1999). A geostrophic transport estimate for the Florida Current from the oxygen isotope composition of benthic foraminifera. *Paleoceanography*, *14*(3), 360–373. https://doi.org/10.1029/1999PA900001

Lynch-Stieglitz, J., Schmidt, M. W., Gene Henry, L., Curry, W. B., Skinner, L. C., Mulitza, S., et al. (2014). Muted change in Atlantic overturning circulation over some glacial-aged Heinrich events. *Nature Geoscience*, *7*(2), 144–150. https://doi.org/10.1038/ngeo2045

Lynch-Stieglitz, J., Valley, S. G., & Schmidt, M. W. (2019). Temperature-dependent ocean–atmosphere equilibration of carbon isotopes in surface and intermediate waters over the

deglaciation. *Earth and Planetary Science Letters*, *506*, 466–475. https://doi.org/10.1016/j.epsl.2018.11.024

Marchitto, Thomas M., & Broecker, W. S. (2006). Deep water mass geometry in the glacial Atlantic Ocean: A review of constraints from the paleonutrient proxy Cd/Ca. *Geochemistry, Geophysics, Geosystems*, *7*(12). https://doi.org/10.1029/2006GC001323

Marchitto, T.M., Curry, W. B., Lynch-Stieglitz, J., Bryan, S. P., Cobb, K. M., & Lund, D. C. (2014). Improved oxygen isotope temperature calibrations for cosmopolitan benthic foraminifera. *Geochimica et Cosmochimica Acta*, *130*, 1–11. https://doi.org/10.1016/j.gca.2013.12.034

Marchitto, T.M., Bryan, S. P., Doss, W., McCulloch, M. T., & Montagna, P. (2018). A simple biomineralization model to explain Li, Mg, and Sr incorporation into aragonitic foraminifera and corals. *Earth and Planetary Science Letters*, *481*, 20–29. https://doi.org/10.1016/j.epsl.2017.10.022

Marcott, S. A., Clark, P. U., Padman, L., Klinkhammer, G. P., Springer, S. R., Liu, Z., et al. (2011). Ice-shelf collapse from subsurface warming as a trigger for Heinrich events. *Proceedings of the National Academy of Sciences*, *108*(33), 13415–13419. https://doi.org/10.1073/pnas.1104772108

Martínez-Botí, M. A., Marino, G., Foster, G. L., Ziveri, P., Henehan, M. J., Rae, J. W. B., et al. (2015). Boron isotope evidence for oceanic carbon dioxide leakage during the last deglaciation. *Nature*, *518*(7538), 219–222. https://doi.org/10.1038/nature14155

McManus, J. F., Francois, R., Gherardi, J.-M., Keigwin, L. D., & Brown-Leger, S. (2004). Collapse and rapid resumption of Atlantic meridional circulation linked to deglacial climate changes. *Nature*, *428*, 834.

Menviel, L., Spence, P., & England, M. H. (2015). Contribution of enhanced Antarctic Bottom Water formation to Antarctic warm events and millennial-scale atmospheric CO2

increase. *Earth and Planetary Science Letters*, *413*, 37–50. https://doi.org/10.1016/j.epsl.2014.12.050

Menviel, L., Spence, P., Yu, J., Chamberlain, M. A., Matear, R. J., Meissner, K. J., & England, M. H. (2018). Southern Hemisphere westerlies as a driver of the early deglacial atmospheric CO2 rise. *Nature Communications*, *9*(1). https://doi.org/10.1038/s41467-018-04876-4

Middag, R., van Heuven, S. M. A. C., Bruland, K. W., & de Baar, H. J. W. (2018). The relationship between cadmium and phosphate in the Atlantic Ocean unravelled. *Earth and Planetary Science Letters*, *492*, 79–88. https://doi.org/10.1016/j.epsl.2018.03.046

Monnin, E., Indermühle, A., Dällenbach, A., Flückiger, J., Stauffer, B., Stocker, T. F., et al. (2001). Atmospheric CO_2 Concentrations over the Last Glacial Termination. *Science*, *291*(5501), 112–114. https://doi.org/10.1126/science.291.5501.112

North Greenland Ice Core Project members, Andersen, K. K., Azuma, N., Barnola, J.-M., Bigler, M., Biscaye, P., et al. (2004). High-resolution record of Northern Hemisphere climate extending into the last interglacial period. *Nature*, *431*(7005), 147–151. https://doi.org/10.1038/nature02805

Oppo, D. W., Gebbie, G., Huang, K.-F., Curry, W. B., Marchitto, T. M., & Pietro, K. R. (2018). Data Constraints on Glacial Atlantic Water Mass Geometry and Properties. *Paleoceanography and Paleoclimatology*. https://doi.org/10.1029/2018PA003408

Parrenin, F., Masson-Delmotte, V., Kohler, P., Raynaud, D., Paillard, D., Schwander, J., et al. (2013). Synchronous Change of Atmospheric CO2 and Antarctic Temperature During the Last Deglacial Warming. *Science*, *339*(6123), 1060–1063. https://doi.org/10.1126/science.1226368

Pedro, J. B., Jochum, M., Buizert, C., He, F., Barker, S., & Rasmussen, S. O. (2018). Beyond the bipolar seesaw: Toward a process understanding of interhemispheric coupling. *Quaternary Science Reviews*, *192*, 27–46. https://doi.org/10.1016/j.quascirev.2018.05.005

Poggemann, D. - W., Nürnberg, D., Hathorne, E. C., Frank, M., Rath, W., Reißig, S., & Bahr, A. (2018). Deglacial Heat Uptake by the Southern Ocean and Rapid Northward Redistribution Via Antarctic Intermediate Water. *Paleoceanography and Paleoclimatology*, *33*(11), 1292–1305. https://doi.org/10.1029/2017PA003284

Rae, J. W. B., Burke, A., Robinson, L. F., Adkins, J. F., Chen, T., Cole, C., et al. (2018). CO_2 storage and release in the deep Southern Ocean on millennial to centennial timescales. *Nature*, *562*(7728), 569–573. https://doi.org/10.1038/s41586-018-0614-0

Rasmussen, S. O., Bigler, M., Blockley, S. P., Blunier, T., Buchardt, S. L., Clausen, H. B., et al. (2014). A stratigraphic framework for abrupt climatic changes during the Last Glacial period based on three synchronized Greenland ice-core records: refining and extending the INTIMATE event stratigraphy. *Quaternary Science Reviews*, *106*, 14–28. https://doi.org/10.1016/j.quascirev.2014.09.007

Roberts, J., Gottschalk, J., Skinner, L. C., Peck, V. L., Kender, S., Elderfield, H., et al. (2016). Evolution of South Atlantic density and chemical stratification across the last deglaciation. *Proceedings of the National Academy of Sciences*, *113*(3), 514–519. https://doi.org/10.1073/pnas.1511252113

Robinson, R. S., & Sigman, D. M. (2008). Nitrogen isotopic evidence for a poleward decrease in surface nitrate within the ice age Antarctic. *Quaternary Science Reviews*, *27*(9–10), 1076–1090. https://doi.org/10.1016/j.quascirev.2008.02.005

Rosenthal, Y., Lear, C. H., Oppo, D. W., & Linsley, B. K. (2006). Temperature and carbonate ion effects on Mg/Ca and Sr/Ca ratios in benthic foraminifera: Aragonitic species *Hoeglundina elegans*. *Paleoceanography*, *21*(1). https://doi.org/10.1029/2005PA001158

Sarmiento, J. L., Gruber, N., Brzezinski, M. A., & Dunne, J. P. (2004). High-latitude controls of thermocline nutrients and low latitude biological productivity. *Nature*, *427*(6969), 56–60. https://doi.org/10.1038/nature02127

Schlitzer, R. (2015). *Ocean Data View*. Retrieved from https://odv.awi.de/

Schmittner, A., & Lund, D. C. (2015). Early deglacial Atlantic overturning decline and its role in atmospheric CO_2 rise inferred from carbon isotopes ($\delta^{13}C$). *Climate of the Past*, *11*(2), 135–152. https://doi.org/10.5194/cp-11-135-2015

Seierstad, I. K., Abbott, P. M., Bigler, M., Blunier, T., Bourne, A. J., Brook, E., et al. (2014). Consistently dated records from the Greenland GRIP, GISP2 and NGRIP ice cores for the past 104 ka reveal regional millennial-scale δ18O gradients with possible Heinrich event imprint. *Quaternary Science Reviews*, *106*, 29–46. https://doi.org/10.1016/j.quascirev.2014.10.032

Sortor, R. N., & Lund, D. C. (2011). No evidence for a deglacial intermediate water $\Delta^{14}C$ anomaly in the SW Atlantic. *Earth and Planetary Science Letters*, *310*(1–2), 65–72. https://doi.org/10.1016/j.epsl.2011.07.017

Tessin, A. C., & Lund, D. C. (2013). Isotopically depleted carbon in the mid-depth South Atlantic during the last deglaciation. *Paleoceanography*, *28*(2), 296–306. https://doi.org/10.1002/palo.20026

Them, T. R., Schmidt, M. W., & Lynch-Stieglitz, J. (2015). Millennial-scale tropical atmospheric and Atlantic Ocean circulation change from the Last Glacial Maximum and Marine Isotope Stage 3. *Earth and Planetary Science Letters*, *427*, 47–56. https://doi.org/10.1016/j.epsl.2015.06.062

Thiagarajan, N., Subhas, A. V., Southon, J. R., Eiler, J. M., & Adkins, J. F. (2014). Abrupt pre-Bølling–Allerød warming and circulation changes in the deep ocean. *Nature*, *511*(7507), 75–78. https://doi.org/10.1038/nature13472

Weldeab, S., Arce, A., & Kasten, S. (2016). Mg/Ca-$\Delta CO_3^{2-}{}_{\text{pore water}}$–temperature calibration for *Globobulimina spp.*: A sensitive paleothermometer for deep-sea temperature reconstruction. *Earth and Planetary Science Letters*, *438*, 95–102. https://doi.org/10.1016/j.epsl.2016.01.009

Xie, R. C., Galer, S. J. G., Abouchami, W., Rijkenberg, M. J. A., De Jong, J., de Baar, H. J. W., & Andreae, M. O. (2015). The cadmium–phosphate relationship in the western South Atlantic — The importance of mode and intermediate waters on the global systematics. *Marine Chemistry*, *177*, 110–123. https://doi.org/10.1016/j.marchem.2015.06.011

Yu, J., & Elderfield, H. (2008). Mg/Ca in the benthic foraminifera *Cibicidoides wuellerstorfi* and *Cibicidoides mundulus*: Temperature versus carbonate ion saturation. *Earth and Planetary Science Letters*, *276*(1–2), 129–139. https://doi.org/10.1016/j.epsl.2008.09.015

Yu, J., Day, J., Greaves, M., & Elderfield, H. (2005). Determination of multiple element/calcium ratios in foraminiferal calcite by quadrupole ICP-MS. *Geochemistry, Geophysics, Geosystems*, *6*(8). https://doi.org/10.1029/2005GC000964

Yu, J., Elderfield, H., Greaves, M., & Day, J. (2007). Preferential dissolution of benthic foraminiferal calcite during laboratory reductive cleaning. *Geochemistry, Geophysics, Geosystems*, *8*(6). https://doi.org/10.1029/2006GC001571

Zhang, J., Liu, Z., Brady, E. C., Oppo, D. W., Clark, P. U., Jahn, A., et al. (2017). Asynchronous warming and $\delta^{18}O$ evolution of deep Atlantic water masses during the last deglaciation. *Proceedings of the National Academy of Sciences*, *114*(42), 11075–11080. https://doi.org/10.1073/pnas.1704512114

Zhu, J., Liu, Z., Zhang, X., Eisenman, I., & Liu, W. (2014). Linear weakening of the AMOC in response to receding glacial ice sheets in CCSM3. *Geophysical Research Letters*, *41*(17), 6252–6258. https://doi.org/10.1002/2014GL060891

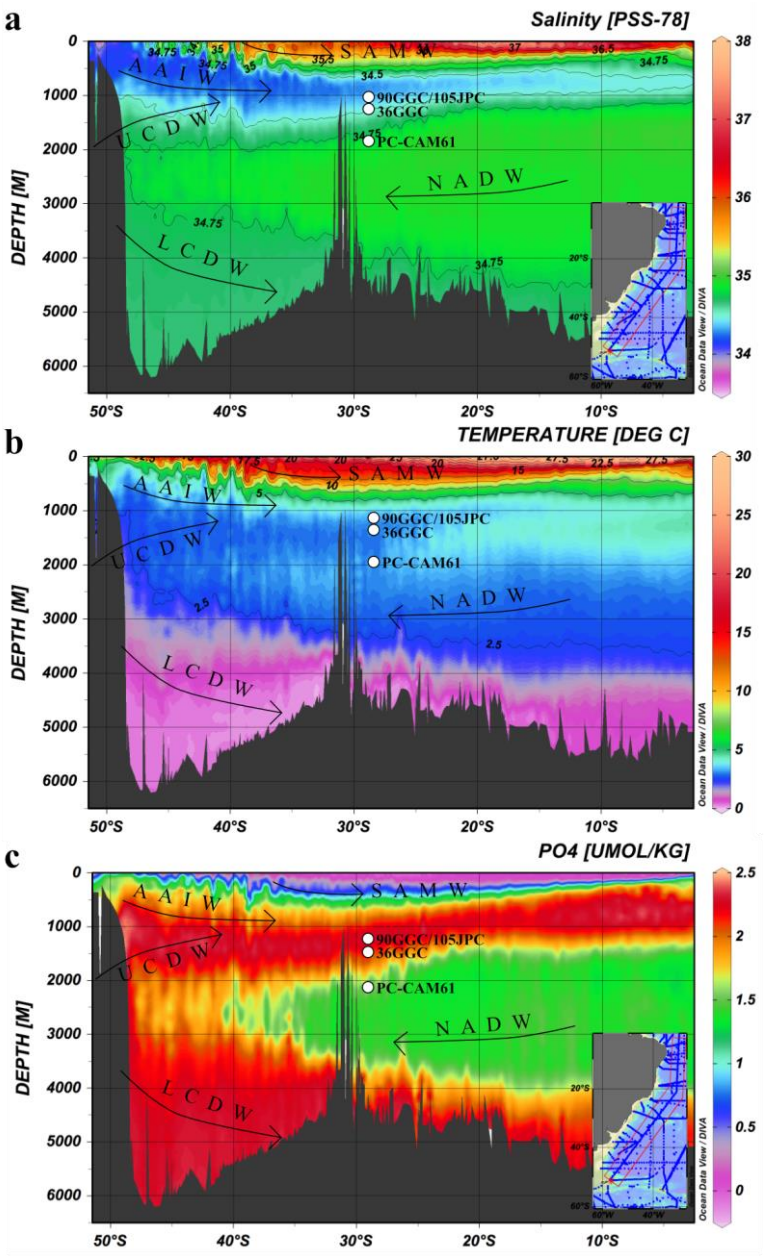

Figure 1. Locations of South Atlantic cores included in this study overlain on a southwest Atlantic cross section (A17) of **(a)** salinity **(b)** temperature and **(c)** phosphate from the World Ocean Circulation Experiment (WOCE) and compiled by the Global Ocean Data Analysis Project version 2.2 (Key et al., 2004). The maps were generated using the Ocean Data View software (Schlitzer, 2015).

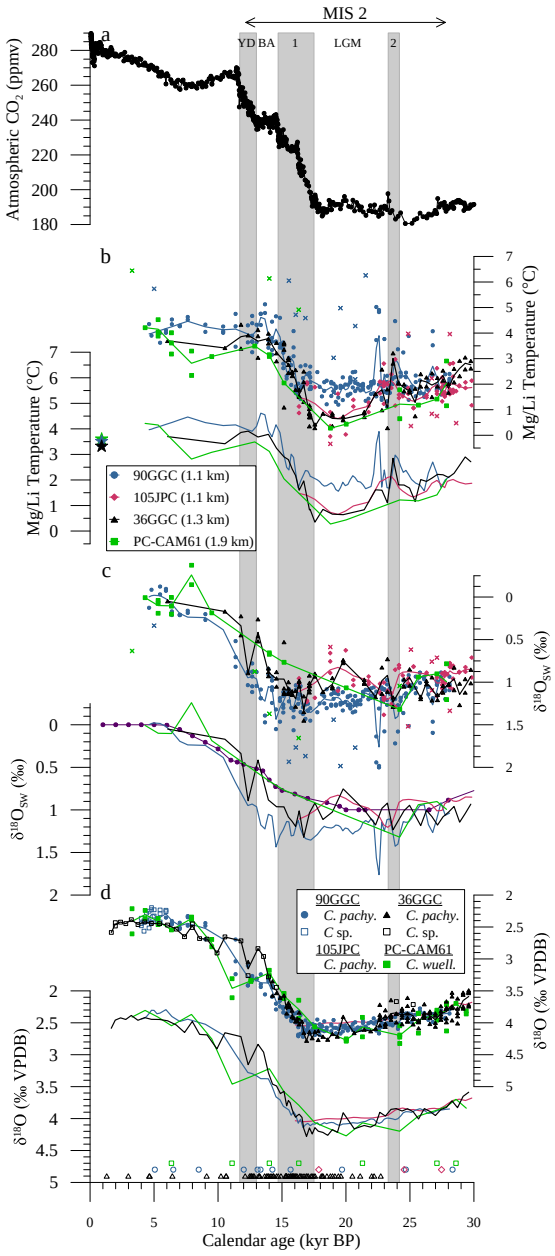

Figure 2. (a) Atmospheric CO_2 (Bereiter et al., 2015) compared to estimated **(b)** BWT, **(c)** $\delta^{18}O_{sw}$, and **(d)** $\delta^{18}O$ from 90GGC, 105JPC, 36GGC, and PC-CAM61. **(c)** Estimates of global mean $\delta^{18}O_{sw}$ changes (purple; Clark et al., 2009) compared to South Atlantic estimates. For the highest resolution cores (90GGC and 105JPC) a local polynomial regression fit and shaded ± standard errors were estimated using the stats package R (Loess). Modern core site BWTs are indicated by stars. Age of calibrated ^{14}C ages used for chronological constraint are indicated along the x-axis by open symbols. Heinrich stadials are numbered and key events labeled at the top.

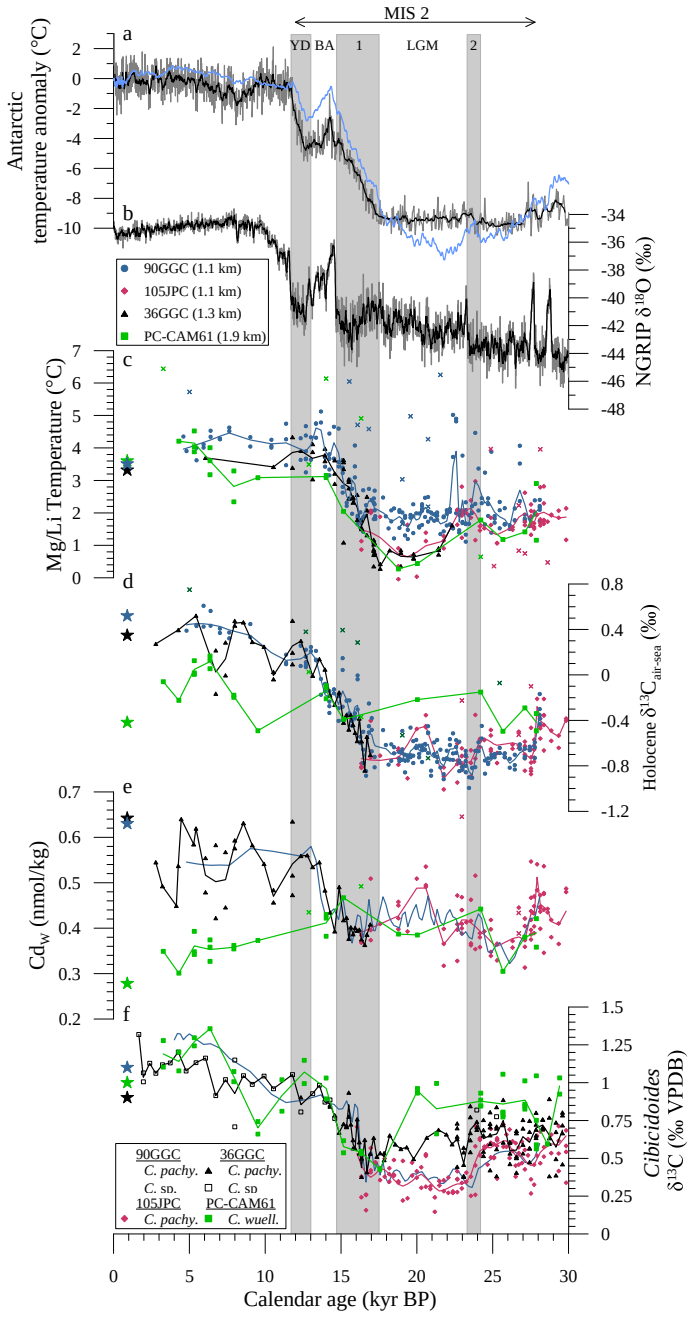

Figure 3. (a) Antarctic temperature anomalies from the EPICA Dome C (Jouzel et al., 2007; black) and West Antarctic Ice Sheet Divide (Cuffey et al., 2016; light blue) ice cores and **(b)** NGRIP Greenland ice core $\delta^{18}O$ (NGRIP members, 2004; Rasmussen et al., 2014; Seierstad et al., 2014) are compared to estimated **(c)** BWT, **(d)** $\delta^{13}C_{air\text{-}sea}$, **(e)** Cd_W, and **(f)** $\delta^{13}C$ for the Brazil Margin (36GGC Cd_W estimates are from Came et al., 2008). $\delta^{13}C_{air\text{-}sea}$ values were estimated using the Holocene equation of $\delta^{13}C_{air\text{-}sea}$ for PO_4>1.3 (Equation 7). Although we can estimate glacial and Holocene $\delta^{13}C_{as}$ (Figure 5) the deglacial evolution between these curves is uncertain.

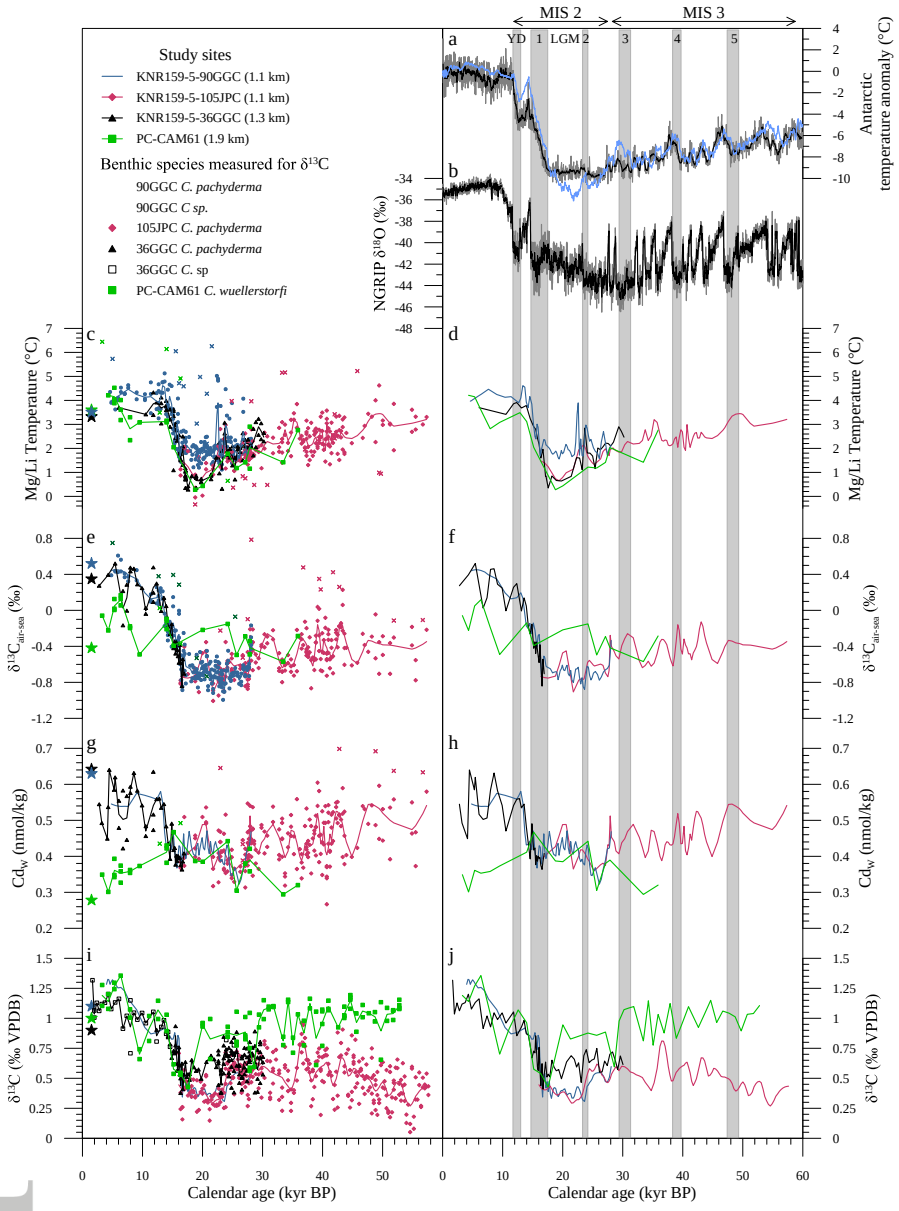

Figure 4 Comparison of **(a)** Antarctic temperature anomalies from the EPICA Dome C (Jouzel et al., 2007; black) and West Antarctic Ice Sheet Divide (WAIS) ice core (Cuffey et al., 2016; light blue) and **(b)** oxygen isotopes from the NGRIP Greenland ice core (NGRIP project members, 2004) on the GICC05 chronology (Rasmussen et al., 2014; Seierstad et al., 2014) to estimated **(c-d)** temperature, **(e-f)** $\delta^{13}C_{air\text{-}sea}$, **(g-h)** Cd_W, and **(i-j)** $\delta^{13}C$ from 90GGC, 105JPC, PC-CAM6, and 36GGC (Came et al., 2008) over the last 60 kyr. $\delta^{13}C_{air\text{-}sea}$ values were estimated for 90GGC using the Holocene equation of $\delta^{13}C_{air\text{-}sea}$ for PO_4>1.3 (Equation 7). Solid lines were estimated by a local polynomial regression fit using the stats package R (Loess), shaded intervals indicate the ±1 standard error of the fits. Data points that were suspected to be influenced bioturbation or contamination (see methods) were not included in the fits (X's). Modern core site values estimated from water column bottle data are indicated by stars.

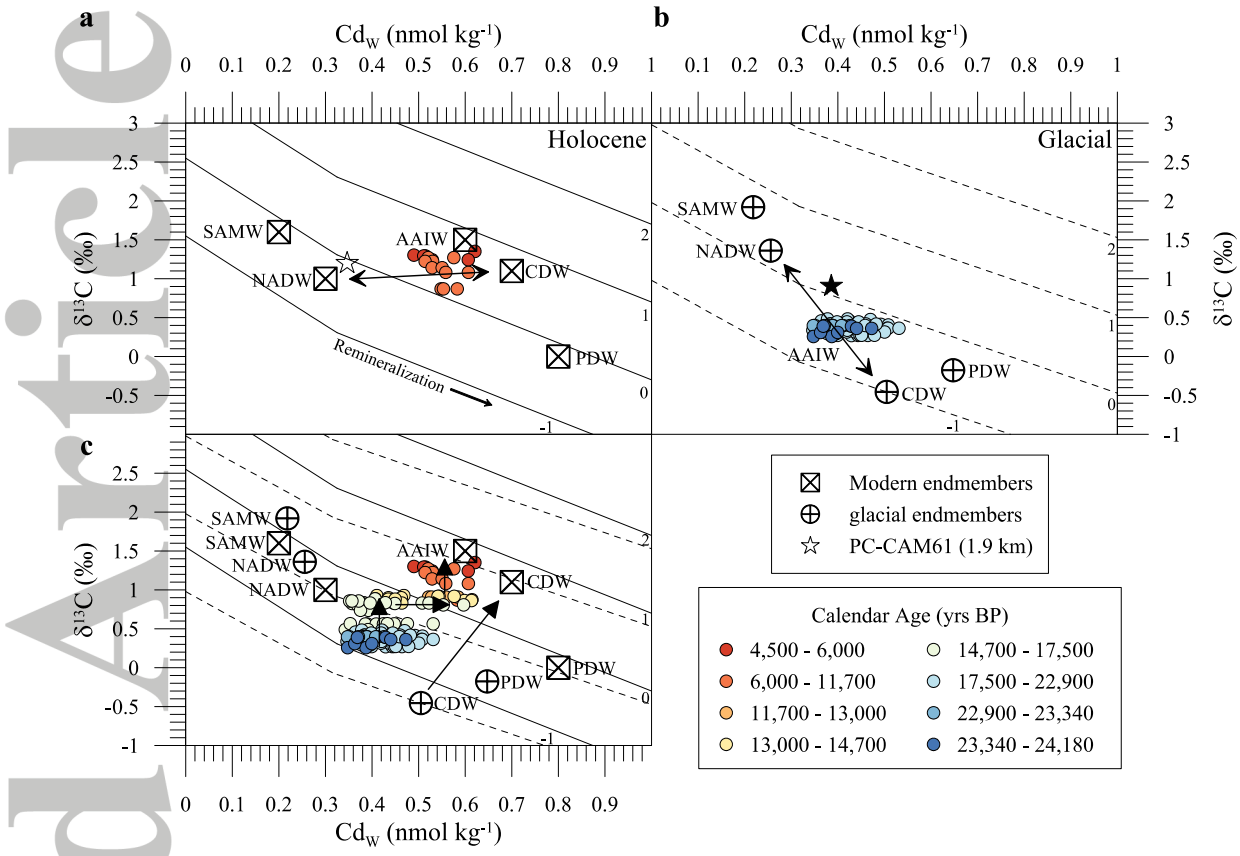

Figure 5. Properties of AAIW from 90GGC Cd_W and $\delta^{13}C$ values are indicated by filled circles with colors corresponding to **(a)** Holocene, **(b)** glacial, and **(c)** deglacial ages. Modern endmember values are from estimated preindustrial $\delta^{13}C$ (Eide et al., 2017) and Cd endmembers estimated from the GEOTRACES GA02 transect (Middag et al., 2018). The Pacific Deep Water (PDW) Cd endmember was estimated from the GEOTRACES GP16 transect (John et al., 2018). Glacial endmembers were estimated from the Cd_W and $\delta^{13}C$ of Boyle (1992), Lynch-Stieglitz et al. (1996), and Marchitto and Broecker (2006). Mean Holocene and LGM values for PC-CAM61 are indicated by open and closed symbols, respectively. Lines of equal $\delta^{13}C_{as}$ were estimated using the Holocene (solid lines) and glacial (dashed lines) using equations 6-9.

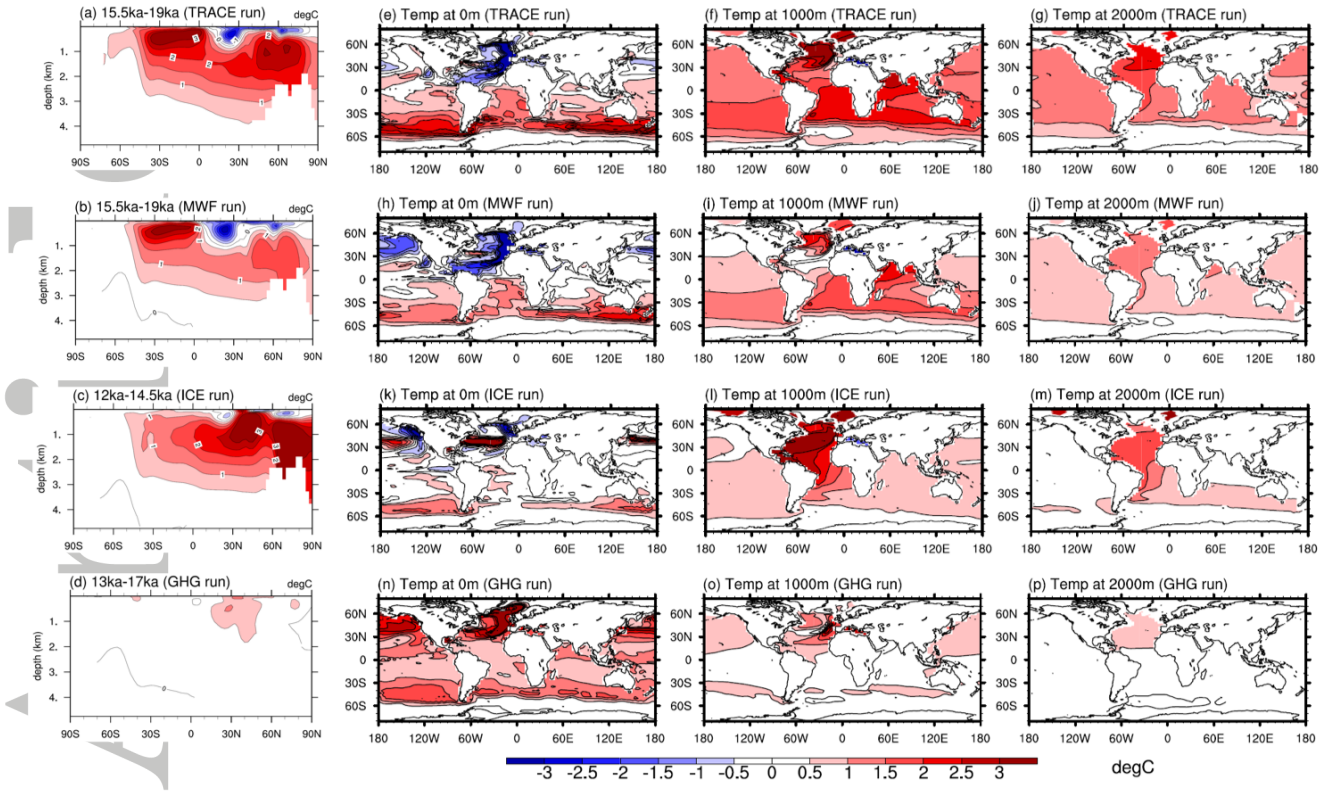

Figure 6. Atlantic cross section (a-d) and map view (e-p) of the surface, 1,000 m and 2,000 m temperature anomalies for the TRACE (first row) and MWF (second row) runs at 15.5-19 kyr BP, the ICE (third row) run at 12-14.5 kyr BP and the GHG (fourth row) run at 13-17 kyr BP from the National Center for Atmospheric Research Community Climate System Model version 3 (NCAR CCSM3; Liu et al., 2009).

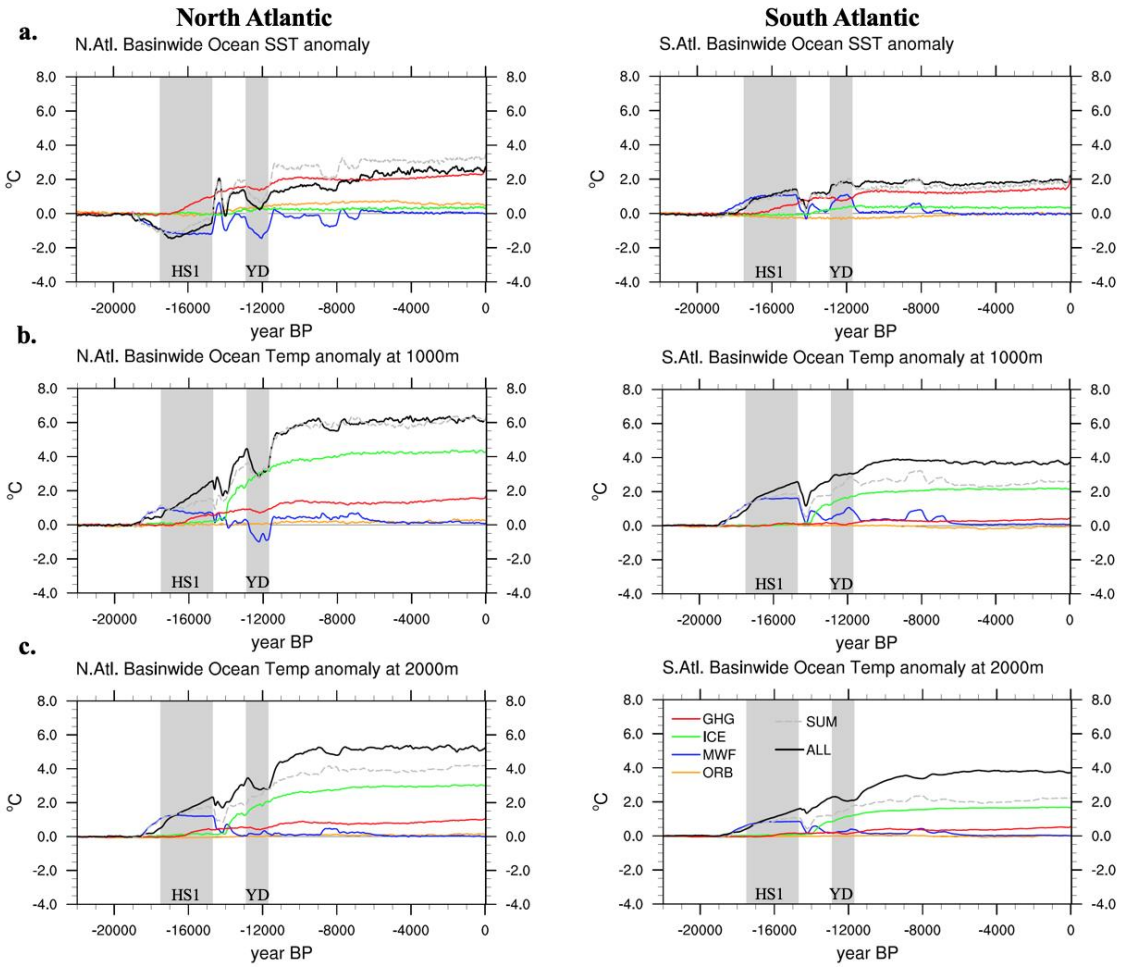

Figure 7. Time series for TRACE, single forcing runs, and their sum, for the North and South Atlantic basins at the **(a)** surface, **(b)** 1,000 m, and **(c)** 2,000 m from the NCAR CCSM3 (Liu et al., 2009).